Multi-domain Vibrations Response of Externally Excited Fluid Conveyer Pipe in Industrial Steam Generator

M. I. Adam [1] * (iD) , **A. Azizan** [1] (iD)

1. Formally, at Department of Mechanical Engineering, NEU, Malaysia.

ABSTRACT

Electric power is an indispensable consumer commodity for a little over a century now as all electric equipment in dwellings, commercial, and industry sectors are essentially dependent on electricity. Heat recovery steam generator, HRSG is an important system in combined cycle power plants. Indeed, excess vibrations induced on such devices may gradually lead to fatigue failure that affect the process of power output. This work investigates, models, and simulates the vibrations response of a fluid carrier pipe housed inside the cavity of the system while experiencing highly pressurized nearly perpendicular external force of extremely hot flue gas on the outside and pressurized water and water vapor from the inside. Transient and steady-state vibrations from initial conditions and the forcing function analysis are performed to account for the variation of damping, amplitude, and frequency responses of the system. Initial parameters used in the systems' model are from industry subsequent to the OEM instructions. However, we introduce a new set of parameter values to observe the vibrational behavior by varying these parameters. The purpose of performing a parameter-based vibration analysis is that parameter variation may point to different responses in the system. Indeed, this in turn indicates which set of parameters are suitable for rectifying the primary causes of undesired vibrations. To account for the consequence of mass flowrate, the model covers low pressure, intermediate pressure, and high-pressure constituents. The results obtained from the model are for the relationships of amplitude and phase angle as functions of frequency of the system. From these data, different interactions of quantities such as force, damping ratio, and number of dampers and vibration supports are observed. These results implore the implementation of new set of parameters to improve the agility of the system and minimize the impact of excess vibrations.
Keywords: HRSG; mass flowrate; pipe vibration.
.

Keyword: HRSG, Mass flowrate, Pipe vibration

INTRODUCTION

Electric power consumption in various industrial plants, hospitals, schools, and every other human dwelling has been a necessity of living in most parts of today's world because all appliances in use require electricity as the main source of energy. Generation of electricity has a variety of sources ranging from non-renewable to renewable ones. Gas turbine combined cycle power plant is one of the most efficient power generating plants because it uses gas and steam turbine that produces 50% more electricity compared to the traditional simple-cycled plants [1-6]. These systems encompass gas turbine, heat recovery steam generator, HRSG, and a steam cycle.

The main purpose of the HRSG in a power plant is its use in energy recovery. By using the extremely hot flue gas from the exit of the gas turbine, a steam cycle can be generated by passing water through the HRSG piping assembly[1-6].

Using this clean exhaust gas from the turbine, the water tube boilers with extended surface are fittingly positioned for heat recovery applications. The higher the inlet gas temperature to the HRSG unit would result in higher amount of steam generated in the HRSG tubes. Because of the large ratio of gas to steam flow, the HRSG is usually huge in size when compared to the size of the packaged boiler that generates equivalent amount of steam. Therefore, exhaust gas flow from gas turbine into HRSG remains nearly constant. Several methods have been presented in literature vis-à-vis modelling the HRSG systems. Dumont *et al*.[7] used a thermodynamic model and mathematical formulation to discuss the heat transfer and pressure drop in the HRSG. Referring to the IAPWS industrial formulation for thermodynamic properties of water and steam, a simulation model was performed using VALI III Software. However, Plis et al [8-11] have shown that mathematical model could be defined using physical and empirical approaches. The empirical method creates a balance model for equations of mass, energy, and heat transfer. NELDER-Mead Simplex optimization algorithm is employed to simulate double pressure HRSG. Aklilu *et al*.[11] used mathematical model to investigate the thermodynamic laws, mass conservation, maps, and empirical simulation. For HRSG systems, the balance model is utilized to analyze other findings in a similar fashion to the analysis made by Peyman *et al*.[12]. While the authors of Ref.[11] focused on developing a mathematical model, authors of Ref.[12] solved the optimization problem by introducing genetic algorithm. Ali *et al*. [13] performed an exergy analysis and obtained the maximum attainable work and economic analysis for cost issues. Data for heat transfer and pressure drop is used to determine the optimum design of HRSG. Bracco *et al*. [14] used MATLAB Simulink for numerical calculations, and Maple Software for the analysis of dynamics behavior and simulated the water level as demonstrated in a phase diagram plot. Alobaid *et al*. [15, 16] used commercial software package APROS by VTT, Finland, to build the static and dynamic simulation of the HRSG during load change and start up. Balance model for energy and mass equations is utilized to observe the flow velocity with different parameters and the influence of fast gas on the entire simulation model. While the result in [16] focuses on the data during load change and start up, analyses the fast hot, warm, and cold startups modes of operation.

Extraordinary vibrations have been observed in HRSG tubes due to fluid flow passing through their normal direction. Flow velocity, which is normally proportional to tube size, causes the tube to vibrate due to exerted flow force [17-19]. It was pointed out that the most problematic vibration mechanism is fluid-elastic instability. Goyder [17] used many vibration mechanisms as a checklist during investigation of system's mechanical integrity. Checklist criteria were fluid-elastic instability, vortex shedding, multi-phase buffeting, acoustic resonance, turbulence buffeting, hydraulic transient, environmental excitation, and transmitted mechanical vibration. Likewise, several other techniques have been devised to investigate the vibrations behavior of the HRSG system [20-23]. The intent of these techniques is to cover all parameters contributing to better comprehension of vibration responses through vigorous

analytical steps. These steps include flow distribution calculations, dynamic parameters evaluation, and formulation of excitation mechanisms, vibration response prediction, and damage assessment.

In case of the HRSG failure, there are two possibilities specified on the Original Equipment Manufacturer, OEM manual. First, the gas turbine coupled to a failed HRSG may operate as simple cycle if the gas turbine passes the environmental license for that specific condition. Second, the gas turbine coupled to the failed HRSG shuts down forcefully. The consequence of both conditions is reduction in power production [7]. HRSG requires high-speed liquid movement with high pressure. Although there are relief valves to control excessive pressure, there still be the high-pressurized motion of liquids and gasses which may cause tube damage if not controlled [23] . In addition, the components within the HRSG system may also weaken due to fatigue, creep, and corrosion. This in turn causes high-amplitude vibration despite the implementation of regular maintenance and parameters checking via instructions of the OEM [7]. Therefore, the resulting vibration developed in the system may increase if the root cause of it is not solved before it causes a complete fatigue failure and tube sagging. Due to large size of HRSG, interrelated vibration complications are unavoidable. Designers of these systems normally perform some meticulous analysis to gauge any possibility of excess vibration occurrences. Two types of vibrational problems may intermix. Because of crossflow, whirling instability of the tubes occurs when the flow velocity inside the tubes exceeds its critical value. This is extremely damaging for the reasons that the HRSG tubes may collectively vibrate in an elliptical form having a single orbit. The resulting fretting wear may consequently push the tubes to impact each other or against their support or hit the shell of the cavity. Fatigue due to over use may also lead to tube attachments to permit failure. The second vibration is resonance due to vortex-induced acoustics or periodic vortex shedding. Flow velocity over tubes, tube diameter, and spacing between adjacent tubes are all parameters contributing in various extends to vortex shedding frequency. When this frequency coincides with the cavity's frequency, a vortex induced resonance frequency occurs. Manifestation of this resonance is a very loud noise characterized by low frequency. Based on the prescribed objectives, this work embarks on three major scopes. Simulation of the HRSG system is carried out to investigate the causes of vibrations in the system using the manufacturer's input data and the parameters given by the OEM. This work also investigates the vibrational behavior of the system by varying the parameters without much altering the original settings of a combined cycle. Based on results obtained from the parameterized model, this work also proposes an optimal parameter setting to the system. In modeling the HRSG system, coding languages such as Python, and the proprietary MATLAB, ANSYS, and MapleSoft are given tools to help investigate the vibrations behavior in the system. Using one or more degrees of freedom formalisms, we study the vibrational response by generating data for damping, amplitudes, and harmonic forced frequency responses.

MODEL CALCULATIONS

For flow-induced vibration velocity, U_P a single-phase flow is defined in terms of pitch velocity.

$$U_p = (U_\infty P)/(P - D) \tag{1}$$

Where U_∞ is free stream velocity, P is pitch between tubes, and D is tube diameter. Homogenous density ρ, free-stream flow path area A, and free stream mass flux $\dot{m}_\infty$, are defined using the homogenous void fraction [19].

$$\rho = \rho_l\left(1 - \varepsilon_g\right) + \rho_g \varepsilon_g$$

$$U_\infty = \frac{\rho_l \dot{V}_l + \rho_g \dot{V}_g}{\rho A}$$

$$\dot{m}_\infty = \rho U_\infty \tag{2}$$

Deduced pitch mass flux, $\dot{m}_p$, is therefore

$$\dot{m}_p = \dot{m}_\infty \frac{P}{(P-D)} = \rho U_p \tag{3}$$

The dynamic parameters for multi-span heat exchanger tubes are mass, flexural rigidity, and damping. The dominant damping mechanism here is the friction between tubes and tube-supports. In addition, there are three important energy dissipation mechanisms at play. They are viscous damping, frictional damping, and squeeze-film damping. Finally, the damping stiffness and support effectiveness were calculated [20-22].

On the other hand, there are three parameters related to vibration excitation mechanisms in HRSG cavity. Fluid-elastic instability, random turbulence excitations, and periodic wake shedding [20]. However, the most important aspect of vibration excitation is fluid-elastic instability expressed in terms of dimensionless flow velocity, and dimensionless mass-damping parameter for single-phase flow of liquids or gasses. The relationships between both parameters is given as:

$$\frac{U_{pc}}{fD} = K \left(\frac{2\pi\xi m}{\rho D^2}\right)^{\frac{1}{2}} \tag{4}$$

where U_{pc} is the critical flow velocity for fluid-elastic instability, $K = 3.0$ is fluid-elastic instability constant, f is tube natural frequency, m is tube mass per unit length, and ξ is damping coefficient. In addition, due to significance of turbulence flow mechanism in vibration excitation, data were analyzed in search for the upper bound taking into account the normalization of excitation force per unit length. Deflection of an HRGS tube, treated as a fixed-fixed beam undergoing forced vibration has the equation of motion [24].

$$EI \frac{\partial^4 w(x,t)}{\partial x^4} + \rho A \frac{\partial^2 w(x,t)}{\partial t^2} = F(x,t) \tag{5}$$

where E is the Young's modulus of the beam's structural steel material, ρ is density of the material, I is second

moment of the beam cross-section about its natural axis, and A is the cross-section. Superposition of individual eigenvalues or mode shapes yields the total normal response.

$$w(x,t) = \sum_{n=1}^{\infty} w_n(x)q_n(t) \tag{6}$$

Where w_n is the nth modal amplitude, q_n is the nth mode shape or that of the beam ends. The nth natural frequency ω_n of the fixed-fixed beam is

$$\omega_n = (\beta L)^2 \sqrt{\frac{EI}{\rho A L^4}} \tag{7}$$

The value of β can be determined from the boundary conditions of the beam. For a viscously damped case, total vibratory response becomes

$$w(x,t) = \frac{F}{\rho A L} \sum_{n=1}^{\infty} \frac{q(x_n)q(x)}{\omega_n^2 - \omega^2 + j2\xi\omega\omega_n} \tag{8}$$

Where $F(x, t)$ is the externally applied force, and ω is the forcing frequency.

METHOD

The HRSG can be viewed as a system where the heat exchanger is located between the hot air blowing from the gas turbine exhaust and the water fluid flowing from vertically arranged tubes. Hot steam and water tubes are all housed in the heat exchanger cavity. The system heats water into steam and the steam produced runs the steam turbine. This cyclic process is effective in generating electricity and is mostly used in related power plants. The system has some complexity in its piping design such as piping shape, number of fins, pipe size, and crossflow. This complexity in design may possibly affect the rate of water crossflow which can lead to vortex shedding – a damaging source of undesired vibrations.

Vibrational behavior of the HRSG system is investigated utilizing different software packages. The Workbench – a multi-domain modeling and simulation tool under ANSYS is used to construct a schematic diagram of the piping system inside the HRGS cavity and run the simulation. Included in this model were three different components, low pressure (LP), intermediate pressure (IP), and high-pressure (HP). A PTC Creo parametric software has also been used to build the digital drawings of the piping system across the HRSG. Transformation to digital drawings were successfully made by considering few assumptions to overshoot or rather simplify the complexity. Simplification through reasonable assumptions allows for imitation so that the resulting 3D shape of the HRSG system closely resembles the original one. The final aim of the 3D digital model is to estimate the behavior of a real world HRSG system. Completion of modeling process inside the cavity points to two more different types of analysis to undertake. Computational fluid dynamics, CFD software is used to calculate the flowrate, flow velocity, and pressure of the flow force of the flowing gas and the pouring water forces along the inner diameter of the piping system. These two nearly perpendicular forces were later used in the vibration response analysis of the

system. CFD analysis begins with a 3D model in PTC Creo parametric software. The format of the file has been manipulated so that ANSYS-based software can properly read it. The file is then imported into Gambit software for meshing process and specification of boundary conditions. This file later exported onto a mesh file in Fluent software to specify all values of the boundary conditions, type of materials, type of flows, and other parameters such as velocity, pressure, and temperature. Vibration analysis begins after the completion of model schematic diagram in the Workbench platform. This allows automated production of diagram of the HRSG system and the graphical presentations at the end of calculations. Calculation's process encompasses the geometry, modal, and harmonic response.
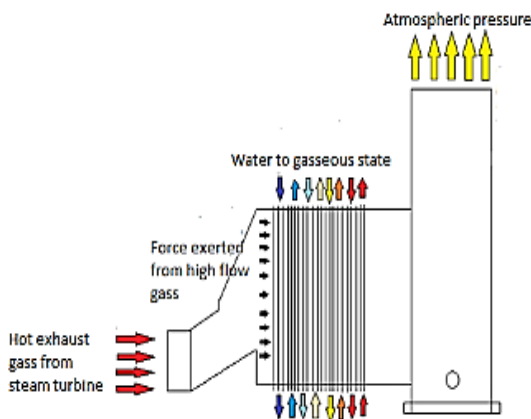
RESULTS and DISCUSSION

The iteration process runs based on the input parameters. Using the given set of equations in the general model setup, the systems' iteration runs until the nth iteration number where all equations converge at a percentage of error of less than 1.0×10^{-2} %. These settings alert about the boundary conditions fed to the model to signal that construction of model, meshing process, and specification of boundary conditions have been successfully read from the mesh file. Figure 1 shows the final mesh model of the HRSG system which has been translated from the schematic drawing shown to the left of Figure1 panel. The blue-coloured section down the left of the meshed 3D HRGS shows the pressure inlet, and the red colour at top right illustrates the outlet section.
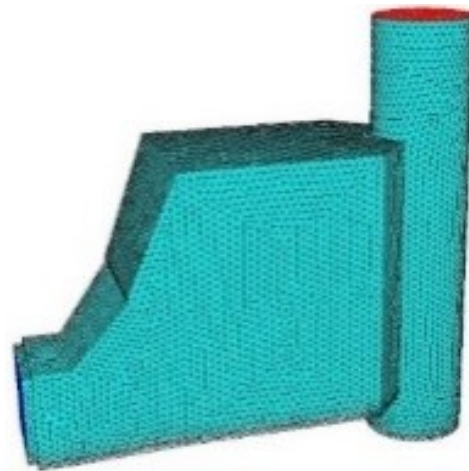

Figure 1: Schematic, and meshed model of the HRSG system scaled to respective units and dimensions. Note that the mesh model dimensions are given in millimeter units.

The meshing process runs through mesh quality observation which allows for identification of the quality of the model as well as its ratings. The orthogonality of meshing quality ranges between 0.0 and 1.0. In this model, the minimum orthogonal quality is ~ 0.7 which symbolizes a good meshing quality. At this point, it is desired to find the pressure difference across the centerline of the HRSG system and the pressure variation across the front row of its piping assembly. The intended pressure in this case is the high-pressure, (HP) across the super-heater pipes. Hence, the turbulent flow is chosen based on the equation of the Reynolds number

$$Re = \frac{\dot{m}D}{A\mu} \qquad (9)$$

where $\dot{m}$ is mass flowrate of the system, D is pipe diameter, A is cross-sectional area at the inlet, and μ is dynamic viscosity of the fluid. Because the inlet opening is square-shaped, expression for the diameter of the inlet obeys the value $D = 4A/p$, with p as perimeter [25]. The analysis process requires specification of character of the materials involved to feed the model equations. The fluids and solids

materials in this system are air, and structural steel, respectively. The lodged boundary conditions are mass flowrate, pressure at the inlet, and atmospheric pressure at the outlet. In this way, the general setup process have been successfully made and the system is now ready to converge a solution via solution method, solution initialization followed by actual calculations. The solution method accepts changes in spatial discretization to initiate the starting point for iteration. The manually set n^{th} number of iterations thereof completes the calculation for all the equations if to converge at a percentage error of less than 1×10^{-2} %. Figure 2 shows the relationships between the percentage errors of the iterations process. The calculation stops at 2000 iterations as specified in the input file. All calculations reaches below $1x10^{-2}$% iterations except for the cavity wall roughness, ε which hovers very close by. At this moment, we concentrate on data extraction. Line approach yields the data of pressure difference across the centerline of the HRSG cavity. Plane approach produces the data of pressure variation at the first row of the pipes. This extraction process also searches for mass flowrate of the system at the inlet and the outlet points.
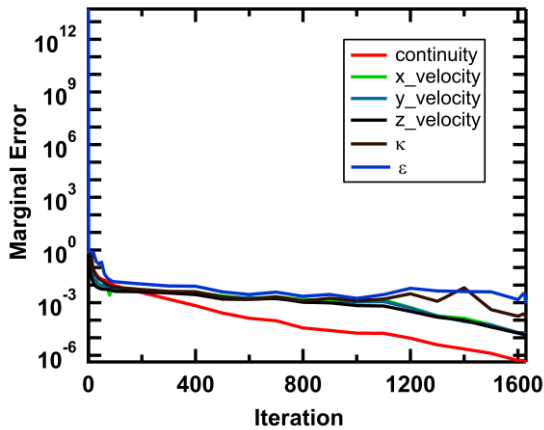
Figure 2: Graph of the iteration process necessary for successful model calculations.

Variations of mass flowrate at the inlet and the outlet produces a small percentage difference. This validates the accuracy of model calculations.

Table 1: Mass flowrate at inlet, and outlet locations. The small value of net mass flowrate indicates the accuracy of the calculation.

Location	Mass flowrate (kg/s)
Inlet	601.1
Outlet	-601.0995
Net mass flowrate	0.0001462

From Table 1, the mass flowrate at inlet, and the outlet locations are almost identical with percentage differences of 2.43×10^{-7}%. This shows that the analysis process of the system is accurate and valid to go through the next stage of data extraction.

The model of the piping system is generated using ANSYS Workbench, which contains the geometry, modal, and harmonic responses, respectively. This also creates an animation of vibrating single pipe and tabulated data on the response of the piping system employing different processing parameters. Selection of a single pipe from the middle of the first row of the piping assembly allows for simplification and practicality of the model. The impact of forces acting on a single pipe also facilitates the interaction between the pipes at the first row and, consequently gives an indication for the cause of fatigue failure. We disregard the lump sum data generated from the completely first row of the piping system since it is not possible to study the interaction between each pipe this way. Instead, the model employs the industry-designed dimensions, geometry, and materials specifications of pipes as default parameters. The default settings of the model is shown in Table 2. The modal section of the model identifies the location of the fixed supports of the vibrating pipe and determines the mode shapes of vibration with different frequencies. The focus at this point is the frequency of the pipe when it is in total deformation state. This frequency feeds the model harmonic response section in order to identify the range of all frequencies. The harmonic response section of the model deals with location-specific forces acting on the system.

Table 2: Parameters of the default settings of high pressure super heater pipe.

Parameter	Values
Length of pipe	17.959 m
Inner diameter of pipe	0.0445 m
Thickness of pipe	0.00584 m
Fin thickness	0.0161 m
Gap between pipes	0.0090 m
Material of pipe	structural steel
Density of material	7850 kg/m^3
Mass flowrate	601.1 kg/s
Flue gas pressure	109.4 Pa
External force due to gas flow	173.6 N
Internal force due to water flow	137.17 N
Damping ratio	~
Number of vibrations supports	~

There are two forces acting on the piping system. External forces due to the flue gas nearly perpendicular to the pipes, and internal force due to the flow of water. A simple expression of $F=PA$ yields the pressure given in terms of force. Since pressure distribution is a common feature in this system, the force generated from such pressure is a distributed force in nature. For the sake of simplicity, it's assumed that the concentration of this force is much higher

towards the center of the pipes. The model treats the internal forces acting inside the pipes as unified gravitational force due to the combined mass of water and water vapor. This is because the piping system is a heat exchanger where water converts to vapor. Therefore, the total volume of force inside the pipe is divided into two parts, water, and vapor with mass $m = \rho V$, and weight $W = mg$. Calculated internal force is 137.17 N. This gives the range of frequency as the total

deformation frequency with a value ranging from 0.0 to 1.5 times of the total deformation frequency. Here, the results obtained from the model settings are for the relationships of amplitude and phase angle to the frequency of the system. From these data, different interactions of quantities such as force, damping ratio, and number of vibration supports are observed.

First, by way of clairvoyance, the flow velocity of hot air must have the greatest effect on the first row of the piping assembly. This is because the first row of the piping is less surrounded by much barriers that may resist the flow. As the flow passes through the first row, the velocity may slightly drop as it experiences resistance due to the first row of piping acting as a barrier. The second criterion is crossflow pressure. This was determined by constructing the pressure difference graph across the center of the HRSG system. Figure 3 shows the pressure difference across the centerline of the HRSG with variation of mass flowrate. As shown in the figure, the pressure difference as a function of length across the cavity has varied with mass flowrate from 400 kg/s to 800 kg/s. All curves have shown nearly identical shape notwithstanding difference in mass flowrate value. This result indicates that the pressure difference is dictated by the shape of the HRSG system inner environment rather than by the variation of the flowrate. It's observed that the highest pressure concentrates at around 10.0 m length across the centerline. Referring to the original drawings, high pressure location is in the vicinity of the front side of the first row of pipes with a variance of about 0.5 m. The observed result indicates that vibration response is significantly active at the vicinity of this location on the piping system.
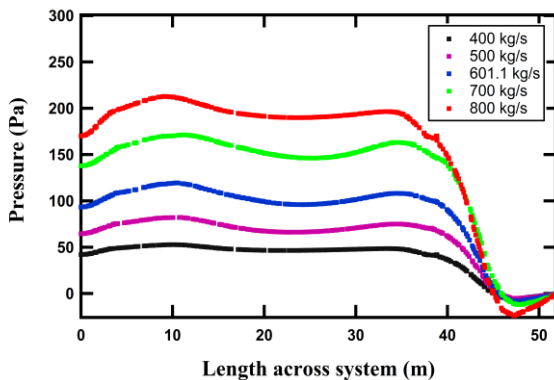
**Figure 3**: Pressure difference across the HRSG cavity with variation of mass flowrate.

From the fundamental concepts of gas flow, the condition at the earlier stages along the system receives high gas pressure while the state of pressure at chimney is atmospheric one. Thus, the gas flow travels faster towards the chimney due to pressure difference. As the distance travelled by the gas flow widens, the pressure across the cavity gradually dips until it reaches the atmospheric pressure. This observation relates to conservation of energy. In a volumetric flow pitch, the Bernoulli equation governs the relationship between pressure, velocity, and position of a fluid particle. Since the water flow inside a pipe have some friction but generally

nonviscous, gravity and pressure are the only external forces acting on it. A fluid is capable of reaching high kinetic energy if its initial state of the liquid is under pressure. For a fluid volume at any two different points a distance apart along the streamline of a uniform circular pipe, the Bernoulli equation gives the following expression for the quantities mentioned above [28]. z_1, z_2 are points in z directional axis.

$$\frac{v_1^2}{2g} + \frac{P_1}{\rho g} + z_1 = \frac{v_2^2}{2g} + \frac{P_2}{\rho g} + z_2 + \sum \frac{fL}{D_h}\frac{V^2}{2g} \tag{10}$$

The sum term indicates that the constant pressure value may drop when many pipes of different diameter are connected together. Manifestation of friction f is either heat loss or internal energy gain for the fluid. On the other hand, research on the thermal efficiency of the HRSG systems focuses on the thermal response of the whole length of the piping assembly. This is simply because the main function of the HRSG is to act as a heat exchanger [12, 13]. Hence, consideration for the whole line of the pipes so as to calculate the thermal efficiency along the length of the pipes. This work did not follow the above-mentioned approach. Instead, we adopt a simple but efficient way to account for temperature gradient in the HRSG system. In addition, the simulation for the whole number of pipes may not be necessary because the first row of pipes experiences the highest pressure while the rest of the pipes arranged backward may experience lesser force of gas flow pressure. Hence, it is deemed adequate to use only the central pipe at the first row in order to draw relative vibrational interpretations.

The mass flowrate is varied through this work in order to observe the most accurate effect obtainable by the system. As the system's pressure relatively weakens inwards, the piping assembly experiences lesser force of mass flowrate compared to the epitome settings. In this case, the mass flowrate becomes the focal cause of vibration thus, reducing this force via damping and supports may minimize the excess vibrations. Pressure force across a single pipe determines the effect of vibration due to mass flowrate. This assertion has been explained briefly in the results section.
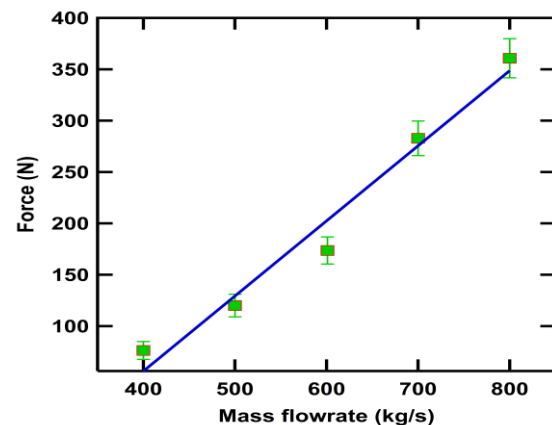

Figure 4: Proportional relationships between forces and mass flowrate.

Figure 4 depicts the relationships between mass flowrate and the forces induced in the HRSG system. This figure acts as a template for additional work to further investigate the observed proportionality between force and mass flowrate in the system. It also permits further determination of forces corresponding to any mass flowrate using the linear relation $y = 0.73x-236.3$, an equation added by performing a linear regression on the response of the system. Form Figure 4, the forces acting on the system increase as the mass flowrate increases. This is due to proportionality between pressure and mass flowrate.

Using the information obtained from this figure, we select the forces related to mass flowrate in the system and use them as parameters in the model of the piping system. The results obtained thereafter are for the amplitude and phase angle as functions of frequency. Therefore, the natural frequency of the system and its variations with different forces are properly observed.

Figure 5 shows a bell-shaped curve which start to increase in amplitude as a function of frequency until the frequency ratio equals 1.0 Hz, then it shows a declining pattern as the frequency increases. Variation of mass flowrate leads to amplitude concentration at the frequency ratio of 1.0 Hz. The amplitude is respectively high at near resonance frequency compared to other frequency variations. Almost 80% of the points on these curves were concentrated at amplitude ratio of 0.2 m and below. The shape of the curves remains similar as mass flowrate varied. The amplitude at natural frequency decreases as the mass flowrate decreases.
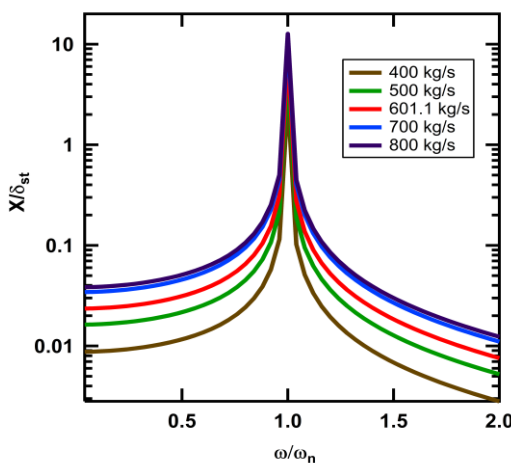

Figure 5: Vibration amplitude as a function of frequency for different mass flowrate.

Throughout the course of analysis, we observe the effect of the harmonic response by varying the damping ratio. The effect of damper installation on the system is verified. Figures 6 and 7 represent the relationships of amplitude ratio and phase angle as a function of frequency ratio.

From Figure 6, the amplitude ratio X/δ_{st}, at the frequency ratio beyond $\omega/\omega_n = 1$ starts to decrease as the damping ratio increases. $\delta_{st} = F_o/k$ is the deflection under the static force F_o. and k is the material spring constant. The steep inclination and visible decline of the curves also decreases as the damping ratio increases. The steepest graph in the figure takes place when the damping ratio $\xi = 0$. However, a

combination of linear and somewhat declining plateau is observed for the damping ratio $\xi = 0.5$. The corresponding amplitude in the graph of damping ratio $\xi = 0.5$ does not exceed 0.05 m.
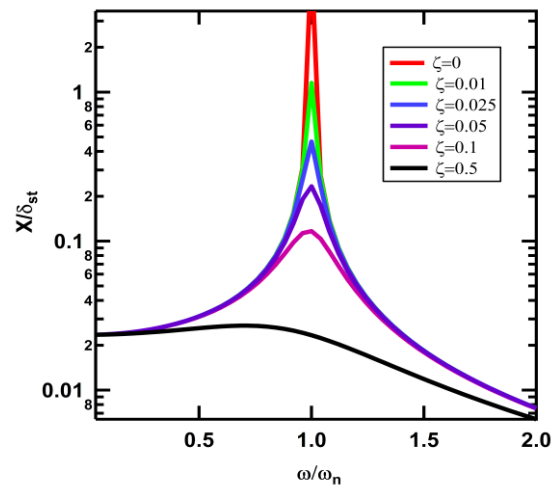
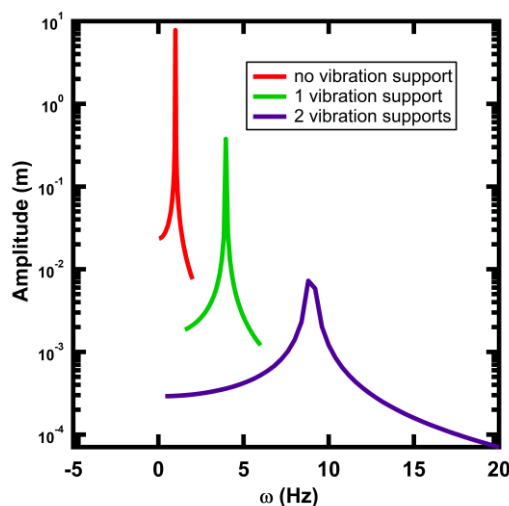**Figure 6**: Relationships between the ratios of amplitude and frequency with variation of damping ratio.

Figure 7 shows the relationships between the phase angle and frequency ratio together with variation of the damping ratio ξ. All the graphs with different mass flowrate show similar behavior. The phase angle starts at 0° until it reaches near the natural frequency before it turns to 90°. The phase angle sharply changes to 180° as it passes through the natural frequency and remains steadily constant as frequency increases when there's no damping on the pipe. Conversely, the phase angle of the system starts to reduce in steepness when approaching the frequency $\omega/\omega_n = 1$ as the damping ratio increases. The steepness starts to reduce as the damping ratio increases and, at the damping ratio $\xi = 0.5$ the curve almost approaches linearity.
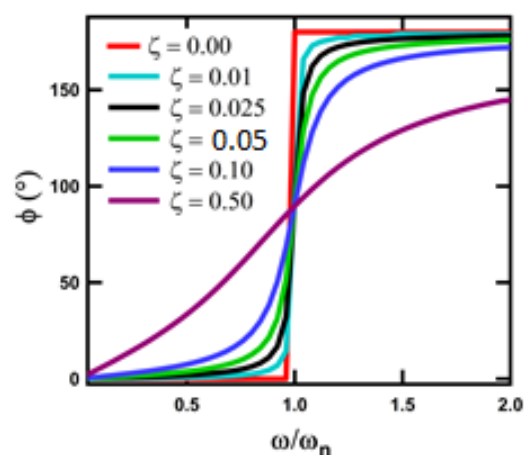
Figure 7: Relationships of phase angle and frequency with varying of damping ratio.

Figures 5, 6, and 7 show similarity in type and shape as that of theoretically calculated forced harmonic vibrations response of undamped/damped system.

For the damped forced system, the reason behind this behavior is that the damping ratio reduces the vibration amplitude of the system. For validation purposes through theoretical methods, the comparison obviously shows clear similarity with the model data. Introduction of a damper with different damping ratio reduces the vibration amplitude of the system over various frequencies and time. This allows the system to vibrate mildly in the acceptable range of frequency. Thus, designers, manufacturers, and operating engineers are less warried about wear and tear or sudden failure of the system. The validity of the information obtained in these figures is theoretically verifiable via methods from the harmonic response and forced vibration of beams. For the undamped case, the damping ratio $\xi = 0$ corresponds to infinite amplitude. This shows a valid verification as the maximum deformation achieved in a pipe of the HRSG system is 6.2 cm while practically, the maximum allowable deformation is actually 4.5 mm as the gap between each pipe is only 9 mm. In the Figure 5-4.7, the maximum amplitude is approximately equal to 5 m at 601.1 kg/s. This amplitude value is already far beyond the maximum deformation, which can be equated to infinity because it is not possible for the pipe geometry to deflect up to that extend. Note that generation of data for this work is based on the geometry of the piping system. In this section,

we retain all parameters from the previous calculations. The exception here is the additional vibration supports to the system. This means the length of the pipe has to be sectioned, depending on the number of vibration supports introduced. The number of vibration supports introduced are 1, and 2 supports, respectively. We attach a single support at the mid-section of the pipe for the first run of calculations followed by two vibrational supports each at a one-third distance along the length of the pipe from both extremes for further analysis. The relationships of the amplitude and phase angle corresponding to the frequency are shown in Figures 8 and 9, respectively. It is obvious that the curves shift to higher frequency side due to the increase of the natural frequency as the number of vibrations supports increases. The behavior for the phase angle is also the same with different value of the natural frequency. The shape of the curves are somewhat different in Figure 8 as the steepness of the graph reduces as the number of vibration support increases. The amplitude at the natural frequency of each curve is also different. There is a decline in the value of the amplitude as the number of vibration support increases. The shape is the same for the relationships of phase angle as a function of frequency. The difference in the location where the phase angle shifts from 0° to 180° now correlates with the value of the natural frequency.

Figure 8: The relationships of amplitude and frequency with variation of number of vibration supports
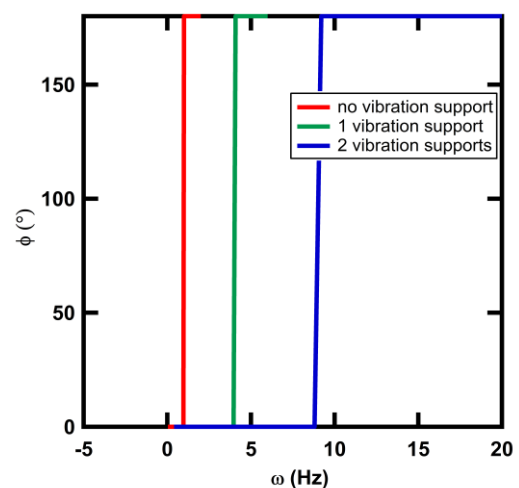
Figure 9: The relationships of phase angle and frequency with variation of vibration supports.

There are two features appearing from Figure 8. They are the reduction on the amplitude at the natural frequency and the shift of the natural frequency. The amplitude of the system decreases as the natural frequency increases. This is because the vibrational forces acting on the system decline according to the number of the vibration supports introduced. When there is no or little vibration support, the distributed forces seemingly concentrate at the center of the system. This feature facilitates for simplification on calculation process because there's only one force acting on the system, which represents the distributed force. In case when a vibration support is in place, the effectiveness of the forces acting at a point of force concentration on the pipe reduces. This leads to dampening of the external forces. As a result, the force

strength decreases and the amplitude of vibration of the system also decreases as a result. The second feature shown in the figure is the shift of natural frequency to higher side of frequency values. It is common practice that introduction of dampers to any mechanical system experiencing undesired vibrations leads to shift of the working frequency away from the near resonance frequency. Hence, the desired natural frequency shifts away to higher frequency as the motion of the mass decreases. Empirically, the spring constant remains the same as there is materials' elasticity relation to the spring constant since all pipes were made of a homogeneous structural steel substance. The above assessment stands proper for the phase angle as a function of shifting frequency due to the effect of vibration supports shown in Figure 9.

Finally, we propose the optimal operating parameters in order to improve the performance of the system. This is because the system initially experiences undesirable vibrations. Our optimized settings focus on the installation of the vibration supports with a good damping ratio. For reasons of a smooth analysis, we keep the mass flowrate as it is. First, the mass flowrate comes from the exhaust of the gas turbine which is coupled with the HRSG. Control of mass flowrate of the system requires further installation of additional chimney or a bypass stack. For the sake of economy, the logical step to improve the system performance is by installation of vibrational supports of good damping ratio instead. Moreover, the system can be installed on the pipe section. Therefore, the main structure remains intact.

Table 3: List of optimal operating parameters.

Parameter	Values
External force (per section)	86.8N
Vibration support	1.0
Damping ratio	0.2

Figure 10 shows a comparison between the initial and optimized parameter settings.
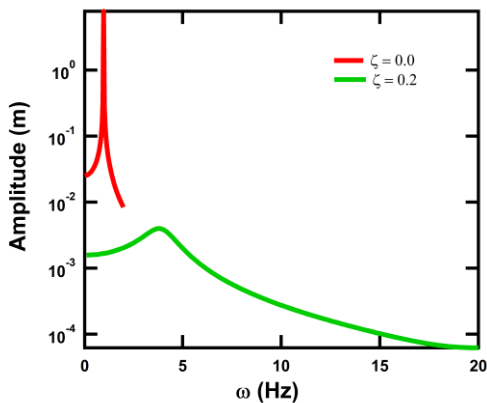
Figure 10: The relationships of the amplitude and frequency for initial, and optimized conditions of the system.

By introducing a single support and the damping ratio $\xi = 0.2$, the maximum vibration amplitude located at the undesired natural frequency shifts away to higher frequency and reduces to 3.97 mm, which is lower than the point of possible friction between any adjacent pipes where the as-built distance is 4.5 mm. Furthermore, the breadth at

different frequencies reduces to very low values averaging at approximately 1.0 mm. The introduction of this vibration support also increases the natural frequency to relocate at 4.0 Hz. This new setting reduces the vibration on the system remarkably thus, increases the life cycle and the reliability of any single pipe throughout the system.

CONCLUSION

An effective modeling and simulation of the HRSG system and the piping system have been established. The model of the HRSG system and piping system was constructed using the ANSYS Fluent and ANSYS Workbench software, respectively. The model showed a good quality on meshing process through which accurate results were obtained. A single pipe from the middle front row of the piping system is analyzed in detail and concise observations were made in regard to the dynamic interaction between pipes. Setting the system to default values, the vibrational behavior is observed through the interactions of amplitude and phase angle with regards to frequency.

So far, three quantities have been drawn from this work. The variation of mass flowrate, the variation of the damping ratio, and the variation of the number of vibrations supports. Data from the model compared to that of the default settings of the system have shown clear differences. Various observations from the implementation of model calculations clearly indicated reduction in excess vibrations occurrence due to introduction of damping forces through vibration supports. The model calculations consequently suggest ways to remedy the existence of undesired variation in the system. Hence, all these parametric variations were suggested for implementation in the new settings in order to improve the system and minimize the impact of excess vibration and possibly avert any unexpected immature failure.

The proposed parameters have been made available based on the analysis and data obtained. In the optimized settings, a vibration support and damping ratio of 0.2 is introduced to the system. The mass flowrate cannot be altered due to the fixed design of the combination of gas turbine and HRSG. To vary the mass flowrate, the bypass stack needed to be installed in the middle between the HRSG and the gas turbine. This is not possible as it costs too much for reconstruction of the combination. The suggested approach is to install vibration supports and vibration damper on the piping system as it is cost effective, nevertheless a minor upgrade to the system

REFERENCES

[1] F. Carazas, C. Salazar, and G. J. E. Souza, "Availability analysis of heat recovery steam generators used in thermal power plants," vol. 36, no. 6, pp. 3855-3870, 2011.

[2] A. Benato, A. Stoppato, and A. J. E. Mirandola, "Dynamic behaviour analysis of a three pressure level heat recovery steam generator during transient operation," vol. 90, pp. 1595-1605, 2015.

[3] N. Petchers, *Combined heating, cooling & power handbook: technologies & applications: an integrated approach to energy resource optimization*. River Publishers, 2020.

[4] A. Ong'Iro, V. Ugursal, A. Al Taweel, and J. J. A. T. E. Walker, "Modeling of heat recovery steam generator performance," vol. 17, no. 5, pp. 427-446, 1997.

[5] G. Electric. Combined cycle power plant: How it works, GE power generation, [Online] [Online]. Available: https://powergen.gepower.com/resources/knowledge-base/combined-cycle-power-plant-how-it-works.html

[6] V. Ganapathy, *Industrial boilers and heat recovery steam generators: design, applications, and calculations*. CRC Press, 2002.

[7] M.-N. Dumont, G. J. C. Heyen, and c. engineering, "Mathematical modelling and design of an advanced once-through heat recovery steam generator," vol. 28, no. 5, pp. 651-660, 2004.

[8] M. Plis and H. Rusinowski, "Mathematical modelling of single pressure heat recovery steam generator," in *Proceedings of the 2015 16th International Carpathian Control Conference (ICCC)*, 2015, pp. 399-404: IEEE.

[9] M. Plis and H. Rusinowski, "Modelling and simulation of the effect of ambient parameters on the performance of a combined cycle gas turbine power plant," in *2016 17th International Carpathian Control Conference (ICCC)*, 2016, pp. 590-595: IEEE.

[10] M. Plis and H. J. I. T. o. I. A. Rusinowski, "Adaptive simulation model of a double-pressure heat recovery steam generator for current optimization in control systems," vol. 53, no. 1, pp. 530-537, 2016.

[11] B. Aklilu and S. J. A. T. E. Gilani, "Mathematical modeling and simulation of a cogeneration plant," vol. 30, no. 16, pp. 2545-2554, 2010.

[12] P. Sindareh-Esfahani, A. Ghaffari, and P. J. A. t. e. Ahmadi, "Thermodynamic modeling based optimization for thermal systems in heat recovery steam generator during cold start-up operation," vol. 69, no. 1-2, pp. 286-296, 2014.

[13] A. Behbahani-Nia, M. Bagheri, and R. J. A. T. E. Bahrampoury, "Optimization of fire tube heat recovery steam generators for cogeneration plants through genetic algorithm," vol. 30, no. 16, pp. 2378-2385, 2010.

[14] S. Bracco, M. Troilo, and A. Trucco, "A simple dynamic model and stability analysis of a steam boiler drum," ed: SAGE Publications Sage UK: London, England, 2009.

[15] F. Alobaid, J. Ströhle, B. Epple, and H.-G. J. A. E. Kim, "Dynamic simulation of a supercritical once-through heat recovery steam generator during load changes and start-up procedures," vol. 86, no. 7-8, pp. 1274-1282, 2009.

[16] F. Alobaid, S. Pfeiffer, B. Epple, C.-Y. Seon, and H.-G. J. E. Kim, "Fast start-up analyses for Benson heat recovery steam generator," vol. 46, no. 1, pp. 295-309, 2012.

[17] H. J. C. E. R. Goyder and Design, "Flow-induced vibration in heat exchangers," vol. 80, no. 3, pp. 226-232, 2002.

[18] M. Pettigrew, C. J. J. o. f. Taylor, and structures, "Vibration analysis of shell-and-tube heat exchangers: an overview—Part 1: flow, damping, fluidelastic instability," vol. 18, no. 5, pp. 469-483, 2003.

[19] M. Pettigrew, C. J. J. o. F. Taylor, and Structures, "Vibration analysis of shell-and-tube heat exchangers: an overview—Part 2: vibration response, fretting-wear, guidelines," vol. 18, no. 5, pp. 485-500, 2003.

[20] S. Khushnood, Z. M. Khan, M. A. Malik, Z. U. Koreshi, M. A. J. N. e. Khan, and design, "A review of heat exchanger tube bundle vibrations in two-phase cross-flow," vol. 230, no. 1-3, pp. 233-251, 2004.

[21] M. Pettigrew, C. Taylor, and N. Subash, "Flow-induced vibration specifications for steam generators and liquid heat exchangers," Atomic Energy of Canada Ltd.1995.

[22] J. C. Jo, M. J. J. N. e. Jhung, and design, "Flow-induced vibration and fretting-wear predictions of steam generator helical tubes," vol. 238, no. 4, pp. 890-903, 2008.

[23] M. Pettigrew, C. Taylor, N. Fisher, M. Yetisir, B. J. N. E. Smith, and Design, "Flow-induced vibration: recent findings and open questions," vol. 185, no. 2-3, pp. 249-276, 1998.

[24] S. S. J. E. A.-W. P. C. Rao, New York, "Mechanical vibrations laboratory manual," 1995.

[25] Y. A. Cengel, S. Klein, and W. Beckman, *Heat transfer: a practical approach*. WBC McGraw-Hill Boston, 1998..